ARL-TR-9477 ● JUNE 2022

DEVCOM ARMY RESEARCH LABORATORY

Electro-Optic Materials Research (Summary Technical Report, 2017–2021)

by Gregory A Garrett and Anand V Sampath

Approved for public release: distribution unlimited.

NOTICES

Disclaimers

The findings in this report are not to be construed as an official Department of the Army position unless so designated by other authorized documents.

Citation of manufacturer's or trade names does not constitute an official endorsement or approval of the use thereof.

Destroy this report when it is no longer needed. Do not return it to the originator.

ARL-TR-9477 ● JUNE 2022

Electro-Optic Materials Research (Summary Technical Report, 2017–2021)

Gregory A Garrett and Anand V Sampath
DEVCOM Army Research Laboratory

Approved for public release: distribution unlimited.

REPORT DOCUMENTATION PAGE

Form Approved
OMB No. 0704-0188

Public reporting burden for this collection of information is estimated to average 1 hour per response, including the time for reviewing instructions, searching existing data sources, gathering and maintaining the data needed, and completing and reviewing the collection information. Send comments regarding this burden estimate or any other aspect of this collection of information, including suggestions for reducing the burden, to Department of Defense, Washington Headquarters Services, Directorate for Information Operations and Reports (0704-0188), 1215 Jefferson Davis Highway, Suite 1204, Arlington, VA 22202-4302. Respondents should be aware that notwithstanding any other provision of law, no person shall be subject to any penalty for failing to comply with a collection of information if it does not display a currently valid OMB control number.
PLEASE DO NOT RETURN YOUR FORM TO THE ABOVE ADDRESS.

1. REPORT DATE *(DD-MM-YYYY)*	2. REPORT TYPE	3. DATES COVERED (From - To)
June 2022	Summary Technical Report	1 October 2017–30 September 2021

4. TITLE AND SUBTITLE
Electro-Optic Materials Research (Summary Technical Report, 2017–2021)

5a. CONTRACT NUMBER

5b. GRANT NUMBER

5c. PROGRAM ELEMENT NUMBER

6. AUTHOR(S)
Gregory A Garrett and Anand V Sampath

5d. PROJECT NUMBER

5e. TASK NUMBER

5f. WORK UNIT NUMBER

7. PERFORMING ORGANIZATION NAME(S) AND ADDRESS(ES)
DEVCOM Army Research Laboratory
ATTN: FCDD-RLS-ED
Adelphi, MD 20783

8. PERFORMING ORGANIZATION REPORT NUMBER
ARL-TR-9477

9. SPONSORING/MONITORING AGENCY NAME(S) AND ADDRESS(ES)

10. SPONSOR/MONITOR'S ACRONYM(S)

11. SPONSOR/MONITOR'S REPORT NUMBER(S)

12. DISTRIBUTION/AVAILABILITY STATEMENT
Approved for public release: distribution unlimited.

13. SUPPLEMENTARY NOTES

14. ABSTRACT
This STR reviews research done on UV avalanche photodiodes (APDs) and LEDs within the electro-optic materials research program FY16–FY21. The initial focus of this work was toward single photon UV detection for compact chemical and biological sensors. This thrust examined approaches for extending the sensitivity of silicon carbide-based APDs into the near-UV and deep-UV spectrums to address applications for bio-fluorescence detection and fluorescence-free Raman spectroscopy, respectively. The second focus was on improving the efficiency of UV LEDs. This work examined carrier transport dynamics in 280-nm UV LEDs and ultimately examined novel nonpolar cubic materials as an approach to increase efficiency.

15. SUBJECT TERMS
STR, UV-Optoelectronics, SiC APD, AlGaN LED, wide bandgap semiconductors, Electromagnetic Spectrum Sciences, Network and Computational Sciences

16. SECURITY CLASSIFICATION OF:			17. LIMITATION OF ABSTRACT	18. NUMBER OF PAGES	19a. NAME OF RESPONSIBLE PERSON
a. REPORT	b. ABSTRACT	c. THIS PAGE			Gregory A Garrett
Unclassified	Unclassified	Unclassified	UU	26	19b. TELEPHONE NUMBER (Include area code) (301) 394-1966

Standard Form 298 (Rev. 8/98)
Prescribed by ANSI Std. Z39.18

Contents

List of Figures

1. Introduction

This report summarizes the main lines of effort for the Electro-Optics Materials Research (EOMR) program including its goals and major accomplishments, focusing on the past 5 years. This EOMR program was an effort within 601102A.31B.1 titled "Optoelectronic and Integrated Photonic Materials and Device Research" for FY16–FY19 and 611102A.AA8.1 titled "Photonic Materials and Device Research" for FY20–FY21. The focus of this EOMR for most of the program was to develop novel semiconductor optoelectronic devices to reduce the size, weight, power, and cost (SWaP-C) of chemical and biological detection and identification systems. Specifically, the program addressed the need for high-sensitivity photodetectors in the near-UV (NUV) spectrum* between 300 and 350 nm for biological agent detection using light-induced fluorescence techniques employed by the Tactical Biological (TAC-BIO) detector, developed by the US Army Combat Capabilities Development Command Chemical Biological Center, as well as in the deep UV spectrum (220–240 nm) important for standoff chemical detection based upon fluorescence-free Raman spectroscopy. Late in the program, this effort pivoted to address assured communications challenges relevant to the Army modernization priority for future networks through examining how to improve the efficiency of solar-blind UV LEDs. This work is divided into four lines of effort summarized in the following and with a more detailed discussion of each of these efforts following within the main report.

1.1 Near-UV Avalanche Photodiodes Based upon Silicon Carbide (NUV-SiC APDs)

The goal of this effort was to demonstrate high-sensitivity APDs using SiC semiconductors that could replace commercially available photomultiplier tubes in the TAC-BIO detector so as to reduce the cost of the sensor by half as well as improve the overall ruggedness of the system. We demonstrated a separate absorption charge multiplication SiC APD with broad responsivity from 200 to 350 nm and gain greater than 106 by successfully addressing the key technical challenge of improving the collection of NUV photogenerated carriers within the device.

* See the Appendix for a detailed explanation of nomenclature for the UV spectrum.

1.2 Deep-UV Avalanche Photodiodes Based upon Silicon Carbide (DUV-SiC APDs)

The goal of this effort was to demonstrate high-sensitivity APDs using SiC semiconductors to replace commercially available intensified charge-coupled device (iCCD) detectors used by standoff chemical detections systems, like the PRIED (Portable Raman Improvised Explosive Detector) developed by Alakai Defense System, so as to greatly reduce SWaP-C. SiC APDs demonstrating multiplication gain greater than 5×10^6 at 12 pW of 240-nm illumination and approximately 12-nA/cm^2 dark current at gain of 1000, suitable for single photon counting, were demonstrated by addressing the key technical challenge of suppressing the effects of surface recombination on the collection of DUV photogenerated carrier within the device.

1.3 Carrier Dynamics in III-Nitride Semiconductor LEDs

To help design more-efficient UV devices, this effort researched the carrier dynamics in these materials through time-resolved photoluminescence (TRPL) techniques supported by modeling using a non-equilibrium Green's function (NEGF) technique. It was shown that the fast photoluminescence (PL) lifetime (how long excited electrons exist before recombining to give off light) observed in these wide bandgap materials could be modeled by a strong excitonic recombination that dominated up to room temperature.[1] The fast PL lifetime was not due to defects but rather the intrinsic radiative lifetime of the device active region. Where the data and model deviated was an indication of localization effects in the active region that could be addressed with device design considerations to improve efficiency.

1.4 Nonpolar Cubic-III-Nitride Semiconductors for LEDs

The idea of this project was to study the relatively unexplored cubic aluminum gallium nitride (AlGaN) material system and investigate its doping properties and radiative emission efficiency to compare its performance against the traditional hexagonal-AlGaN material system. It was learned that heteroepitaxial growth initiation of cubic-AlGaN on the cubic silicon carbide (3C-SiC) using previous processes developed for cubic indium gallium nitride (InGaN) created too many extended defects for useful devices. This problem was attributed to the higher temperature needed for Al incorporations. Possible solutions for future efforts were outlined.

2. Brief Technical Description of Efforts

In this section, a brief description of scientific challenges and results are provided for each focused effort within the EOMR program. Relevant publications with more details are cited wherever applicable.

2.1 NUV SiC APDs

Currently, the responsivity of 4H-SiC APDs reported in the literature peak at approximately 260–270 nm due to loss of photogenerated carriers to surface recombination and weak absorption on the shorter and longer wavelength response, respectively. While this is suitable for replacing the photomultiplier tube within the scatter channel of a bio-fluorescence detector employing a 270-nm LED source,[2] this narrow spectral response prevents the wider insertion of this technology into the fluorescence channel of a bio-fluorescence detector. We have examined these effects in detail by calculating the components of the photoresponse in these devices at unity-gain by analytical solution of the drift-diffusion equation that accounts for surface recombination effects.[3] The results showed that the absorption length for NUV photogenerated carriers is much larger than their bulk diffusion length of approximately 1 μm resulting in poor quantum efficiency. GaN-based APD solutions have been investigated due to strong NUV absorption in this semiconductor, but the dark currents in these devices remain large presumably due to high defect densities.[4] Previously we investigated heterojunction GaN/SiC separate absorption multiplication avalanche photodiodes (SAM-APDs) that would combine the advantages of both materials.[5] However, we found that reproducibly controlling carrier transport at the hetero-interface is difficult.

Instead, in this project we examined a homojunction SiC approach based upon a separate absorption charge multiplication structure, as shown in Fig. 1 (left). This design employs a thick NUV absorption region where carriers can be collected by drift due to a small E-field present therein due to depletion under operation. This is feasible because of the low doping concentrations less than 10^{14} cm^{-3} achievable in 4H-SiC. The measured spectral response as a function of applied bias is shown in Fig. 1 (right). At low bias, the shape of the response is typical of SiC APDs, with a peak quantum efficiency (QE) of approximately 41% at 264 nm. At high reverse bias (~160 V), a significant enhancement in the NUV and DUV response is observed. This results in a relatively flat responsivity of greater than 26 amps per watt (A/W) around 200 nm and from 280 to 360 nm. The improvement in the NUV response with increasing bias is attributed to the expansion of the depletion region with increasing bias and the maximized path of these photogenerated holes through the multiplication region.

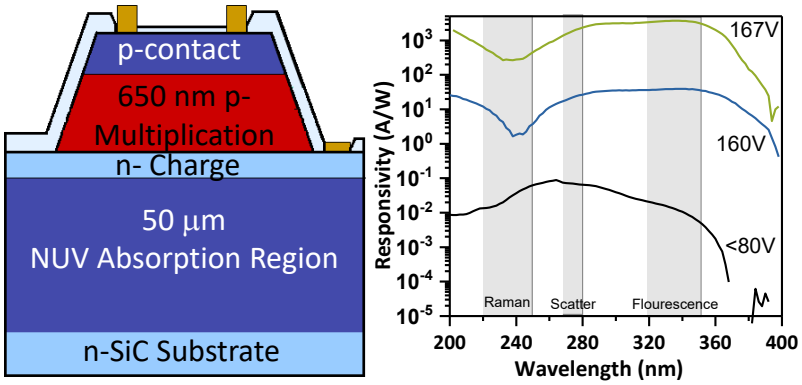

Fig. 1 (left) Structure of UV separate absorption, charge, and multiplication (SACM)-APD and (right) measured photoresponse from SACM-APD showing broad UV response at high reverse bias in spectral ranges relevant for chemical/biological detection and identification applications

The gain at a particular bias in the SACM structure can be calculated by taking the ratio of the photocurrent measured at that bias and at unity-gain. Using this approach, gains of approximately 30×10^6, 2×10^6, and 0.4×10^6 are found at 167-V bias at wavelengths of 370, 350, and 270 nm, respectively. However, the NUV gain calculated in this fashion is not entirely associated with impact ionization because it does not account for the contribution associated with improved collection. Nevertheless, the internal gain in these devices is potentially suitable for Geiger mode operation.

2.2 DUV Enhanced-SiC APDs

High-sensitivity DUV photodetectors operating at wavelengths shorter than 250 nm are essential for applications like resonance Raman spectroscopy-based chemical and biological agent detection and identification, where sensitivity is improved due to both resonance effects[6] and the lack of background fluorescence for photoexcitation in this spectral range. For SWaP-C-constrained environments, room-temperature-operable semiconductor APD arrays are an attractive alternative to the commonly employed cooled-Si iCCDs, which attain large amplification using a microchannel plate, good for UV detection efficiency of approximately 20% and ultra-low dark current (<1 e^-/s).

However, it remains challenging to attain DUV devices with the needed high responsivity, high external QE, and very low dark current (I_{dark}) at gain exceeding 10^6. While AlGaN photodiodes with tunable direct bandgap and peak responsivity in the desired spectral range have been demonstrated,[7,8] Schottky devices[9] and *p-i-n* APDs[10] have achieved gains of only 1.5×10^4 and 1×10^5, respectively, with both the magnitude and voltage dependence of the I_{dark} not conducive to single-photon

counting applications. 4H-SiC APDs, with an indirect bandgap of 380 nm, have exhibited both high UVC[†] (<280 nm) ultraviolet light responsivity[11–13] and high multiplication gain at low I_{dark} density (0.75 nA/cm^2 < J_{dark} < 63 nA/cm^2 at a gain of 1000[14–16]) as well as greater than 10^6 peak multiplication gain.[12,15,17] These properties make SiC APDs very attractive for single-photon counting applications, and 30% single-photon detection efficiency at 280 nm in gated testing has been reported with dark count probability of 8×10^{-4} for 180-µm-diameter devices employing a recessed window.[16] However, the responsivity of these devices diminishes dramatically at wavelengths shorter than 260 nm due to increasing photogeneration of carriers in the top-illuminated doped layer associated with the decreasing UV absorption length, the short effective diffusion length of minority carriers in this region, and the presence of a high density of surface states.

In this effort, we explored approaches to minimize surface recombination effects in 4H-SiC by 1) engineering depletion of the illuminated top layer to improve carrier collection for shorter wavelength excitation by mitigating surface recombination, and 2) leveraging the larger gain for the DUV photogenerated holes due to their maximal path through the multiplication region and the larger ionization rate of holes over electrons. This was accomplished by modifying the doping and thickness of the top illuminated layer so that is substantially depleted at operating bias while maintaining sufficient neutral region thickness to prevent high dark currents associated with punch through, as shown in Fig. 2 top. A blue-shift in peak responsivity is observed for these devices under increasing reverse bias, as shown in Fig. 2 (left). Analytical modeling of the response agrees well with experiment validating the effects of suppressing surface recombination in these structures. APDs with picoWatt sensitivity for 240-nm illumination and with very low dark current (~12 nA/cm^2 at gain of 1,000) were successfully demonstrated, which opens a path for single photon counting in the far UV spectral region, as shown in Fig. 2 right.

[†] Ultraviolet light with wavelengths between 200 and 280 nm

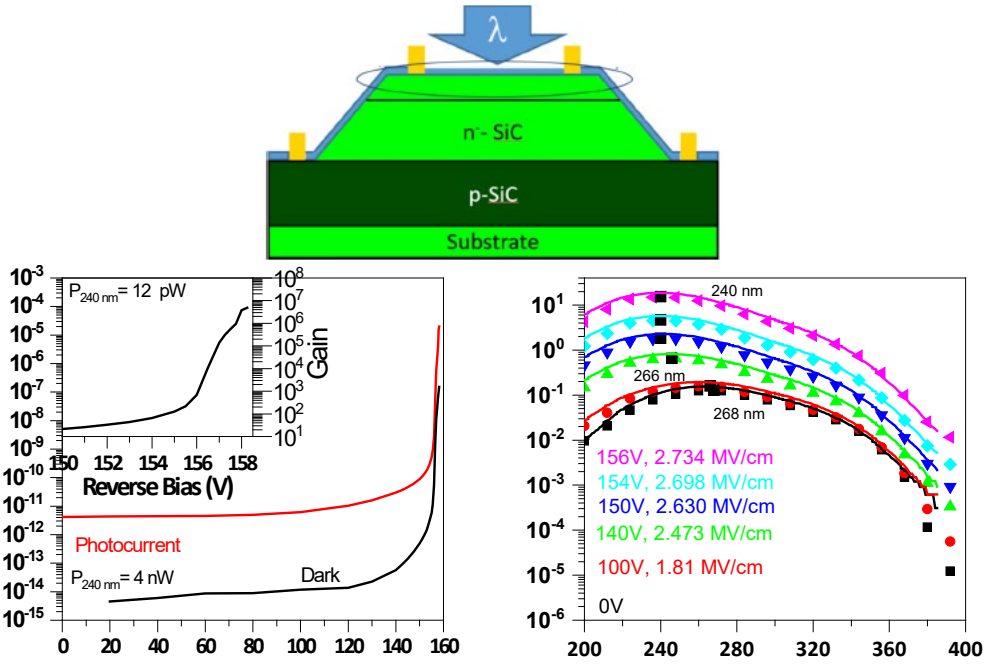

Fig. 2 (top) Device structure for DUV enhanced-SiC APD. (left) Measured photo and dark IV characteristics and calculated gain (inset). (right) Measured (points) and calculated (solid line) photoresponse of SiC APD as a function of reverse bias.

Results show clear inverse relationships observed between the total charge in the top illuminated layer and the maximum blue-shift and dark current density achievable at gain, respectively. However, there appears to be space to extend the limits of these tradeoffs through further design improvements. For example, spiking the doping at the surface of the illuminated contact could prevent punch-through at high bias while also reducing carrier trapping due to surface band bending. One might also consider grading the doping of the top illuminated layer to create a built-in E-field as has been demonstrated recently in Si APDs.[18] Last, the use of AlN as a transparent interface charge control layer can also widen the design space for achieving high gain and low dark currents and shorter wavelengths in these APDs.[19]

2.3 Carrier Dynamics in III-Nitride Semiconductor LEDs

For DUV emitters based on *c*-plan material, the built-in polarization field leads to the separation of electrons and holes in quantum wells and thus a longer radiative lifetimes, the time it takes for an electron and hole to recombine and emit a photon. Long radiative lifetimes can be dominated by shorter nonradiative decays where electrons give up their energy nonradiatively in defects and traps, leading to less-efficient devices with excessive heat generation. This EOMR program made extensive use of a time-resolved optical spectroscopy lab dedicated to excitation

and detection of semiconductor throughout the UV spectrum, 200–400 nm, with 100-fs to 25-ps time resolution to measure these lifetimes. A defining achievement of this program was identifying the fast photoluminescence lifetime of high-quality, high-Al-content AlGaN materials as being a consequence of the expected strong exciton binding energy and not due to nonradiative defects in the material.[1] Note that for high-Al-content materials, the common nonradiative center is oxygen point defects. With this strong understanding of the intrinsic carrier dynamics, the effects of active region design—narrow quantum wells (QWs) to reduce field effects, composition fluctuations from ternary materials, and possibly monolayer well width fluctuations—could be addressed and studied to improve device efficiency.

Integral to understanding the observations made in the TRPL experiments was implementation of a NEGF formalism[20] for modeling the radiative lifetimes of carriers in these materials. Using this model, we were able to calculate the expected radiative lifetime as a function of carrier density and Al content for an $Al_xGa_{1-x}N$ QW. The model, with no a priori experimental inputs, showed a high ratio of excitonic to free carrier recombination, or more importantly, a fast radiative lifetime with a strong carrier density dependence. With the addition of experimental estimates of the nonradiative lifetime, reflecting intrinsic material point defect densities, the model could reproduce measured PL lifetimes with the implication that deviations from the model suggest other carrier localization phenomena (Fig. 3). The work showed the importance of exciton formation in DUV semiconductors and the effects of high carrier density in narrow QW devices (around 2 nm) used in these highly strained emitters to decrease piezoelectric field effects. This model was first developed for the traditional symmetric *c*-plane device orientation and later adapted to non- and semipolar active regions with appropriate approximations to maintain a 1-D calculation. Comparison with experimental TRPL measurements on semi-polar material was favorable. Besides helping design better active regions for DUV LEDs, the understanding provided by TRPL experiments and NEGF modeling will be important for efficient laser designs at these wavelengths, where short radiative lifetimes might conflict with the need for population inversion and longer excited state lifetimes to achieve lasing. These techniques, along with complementary modeling tools developed for wave-function and gain calculations, have been transitioned and are currently being applied to a new program on InGaN-based blue lasers for the quantum-precision navigation and timing (Q-PNT) Essential Research Program.

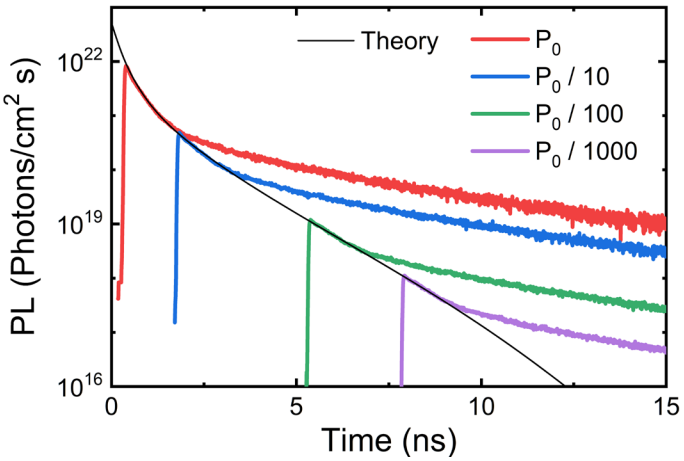

Fig. 3 Representative TRPL of an SET Inc 272-nm LED active region at different excitation densities (color). Deviation from NEGF theory (gray) indicates the presence of other localization phenomenon reducing device efficiency.

Vertical transport modeling was also examined under the EOMR program to help design tunnel junctions for more-efficient hole transport.[21] Tunnel junctions were grown by molecular-beam epitaxy (MBE) on active regions provided through collaboration with University of New Mexico Professor Dan Feezell. Testing these devices showed minimal improvement in device efficiency, and research to improve hole transport was directed toward polarization doping.[22] But the tools developed in this effort have elicited interest from collaborators examining confinement and carrier transport across DUV active regions designed with thin barrier QW well stacks. The EOMR program also identified that being able to model other carrier localization phenomena (monolayer well width fluctuations and alloy inhomogeneity) and their effect on device efficiency would be of benefit to efficient emitter design given the tight binding and dominant fast excitonic recombination shown in DUV emitters.

2.4 Nonpolar Cubic-III-Nitride Semiconductors for LEDs

This line of effort took advantage of a work started under an FY19 Foreign Technology (and Science) Assessment Support program that evaluated 3C-SiC on (001)-Si substrates produced by the UK company KUBOS Semiconductors for cubic-InGaN-based green LEDs.[23] Here, the opportunity presented itself to research the growth and characterization of a new material for wide-bandgap semiconductor optoelectronics, cubic-aluminum-nitride (AlN), and high-Al-content cubic-AlGaN on 3C-SiC substrates. A goal was to ascertain if a certain alloy percentage of cubic-AlGaN might lattice match with cubic 3C-SiC and lead to low-defect heteroepitaxial growth. It was found that due to the higher substrate temperature needed for AlN growth, and due to the thermodynamic stability of the

hexagonal phase over the cubic phase, conditions for initiation of cubic-AlGaN growth were not found. It was concluded that the SiC/Si(001) orientation with a 4° off-cut was not suitable for the growth of cubic-AlGaN due to the presence of dense microtwins along the {111} directions in the initial cubic-GaN epilayer. It was also concluded that continuation of this project should look at other orientations of 3C-SiC such as the (211) surface, which has proved effective in suppressing microtwins in HgCdTe grown on Si(211).[24] With a new SiC machine coming on line at the DEVCOM Army Research Laboratory, Sensors and Electron Devices Directorate (SEDD), Photonics, Electronics & Quantum Sciences (PEQS) Division, a seedling proposal is envisioned to address this idea.

The high-resolution transmission electron microscope (HRTEM) is the most powerful tool to probe the interfacial structure of the crystalline materials. Shown in Fig. 4 is a representative sample of cubic-GaN/SiC/Si grown under our established baseline growth conditions, as examined by the transmission electron microscope (TEM) group led by Dr Wendy Sarney (DEVCOM ARL/SEDD/PEQS), which provides a baseline for comparison of any future efforts. Electron diffraction of the GaN/SiC interface showed good alignment of the GaN epilayer with the cubic-SiC substrate, indicating the crystalline structure of the GaN is indeed zinc blend (cubic). This is supported by observation of the left HRTEM, which shows cubic ABC stacking sequences throughout the GaN layer. However, TEM analysis over a larger area highlights a dense array of microtwins along the crystallography {111} direction initiated at the GaN/SiC interface and extended throughout the entire GaN layer. These microtwins defects can also be viewed as hexagonal inclusions and need to be suppressed for hope of a reasonably performing device.

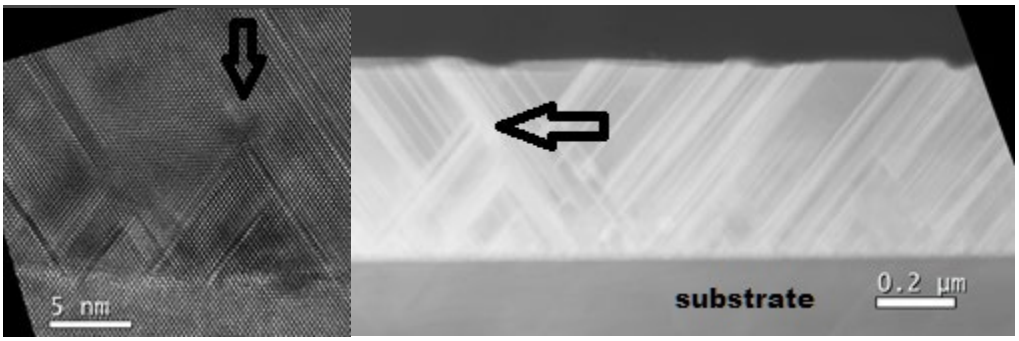

Fig. 4 Cross-section TEM (right) and HRTEM (left) images of a GaN/SiC/Si(001) sample grown by MBE. Bright lines show propagation of defects and domain boundaries from the substrate layer. Arrows show indications of defect annihilation.

3. Conclusion

To address future Army needs for assured communication in an RF-congested and RF-denied environment, efficient UV light sources and high-sensitivity Geiger-mode UV APDs are needed. Given the increasing maturity of the SiC APD effort, we recommend partnerships with industry that can leverage our expertise in device design and testing to accelerate progress in this area. Along these lines, a previously approved FY21 Small Business Innovation Research topic was resubmitted in the current FY22 foundational call.

UV source efficiency affects not just battery life but the interplay between signal range and bandwidth, which defines the use cases for this technology. (This is also true on the detector side of the transceiver.) It is postulated that the Army needs about a 10x improvement over current commercial products for a UVC emitter to even be considered for a Soldier-borne system. The results of this program currently place DEVCOM ARL in a position to quickly address research questions focused on efficient UV emitters. We recommend that the following research ideas be explored in an effort to produce sufficiently efficient UV emitters for a UV radio link:

- Polarization doping for improved carrier injection
- Substrates and substrate preparation for improved light extraction while maintaining active region epilayer quality
- Active region design for highly radiative, excitonic emitters, and related considerations for laser design

While device efficiency is the most important attribute for a UVC emitter for drop-in replacement of the RF channel in a Soldier radio, this program is also wavelength-agile and can address the UVC range of 230–280 nm for assured UV communication. This wavelength agility should be of interest to system designers as they balance the need for transmit distance versus low detection probability, and as they need to factor-in possible malignant effects of UVC on a Soldier because shorter-wavelength UVC tends to be absorbed in the stratum corneum, the outermost epidermal layer consisting of dead cells. We recommend that UVC emitter research cover the full UVC range.

Another interest the resources of this program could address is photonic integrated chip (PIC) development in the near-UV, drawing from recent successes at visible wavelengths (i.e., the Defense Advanced Research Projects Agency's Lasers for Universal Microscale Optical Systems program), for use with alternative quantum systems for PNT, sensing, and information processing as well as higher-power

mid-UV lasers for standoff identification of biological and chemical agents. We recommend exploratory investigation into possible applications of UV PICs and whether they could provide the US Army with a technological overmatch.

4. References

1. Haughn CA, Rupper G, Wunderer T, Yang Z, Johnson NM, Wraback M, Garrett GA. Highly radiative nature of ultra-thin c-plane Al-rich AlGaN/AlN quantum wells for deep ultraviolet emitters. Appl Phys Lett. 2019;114:102101.
2. Cabalo JB, Sickenberger R, Underwood WJ, Sickenberger DW. Micro-UV detector. Proc SPIE. 2004;5617:75–86.
3. Sampath AV, Chen Y, Llopis A, Shen H, Smith J, Kelley S, Wraback M. Enhanced far ultraviolet spectral response and gain in SiC avalanche photodiodes. Appl Phys Lett. 2021;118(22):221102.
4. Dupuis RD, Jae-Hyun R, Shyh-Chiang P, Yoder PD, Yun Z, Jin H, Suk C, Lochner Z. Growth and fabrication of high-performance GaN-based ultraviolet avalanche photodiodes. J Crystal Growth. 2008 Nov;310:5217–5222.
5. Sampath AV, Zhou QG, Enck RW, McIntosh D, Shen H, Campbell JC, Wraback M. P-type interface charge control layers for enabling GaN/SiC separate absorption and multiplication avalanche photodiodes. Appl Phys Lett. 2012;101(9):093506.
6. Tuschel DD, Mikhonin AV, Lemhoff BE, Asher SA. Deep ultraviolet resonance Raman excitation enables explosives detection. Appl Spectr. 2010;4:425.
7. Walker D, Kumar V, Mi K, Sandvik P, Kung P, Zhang XH, Razeghi M. Solar-blind AlGaN photodiodes with very low cutoff wavelength. Appl Phys Lett. 2000;76:403.
8. Butun S, Tut T, Butun B, Gokkavas M, Yu HB, Ozbay E. Deep-ultraviolet $Al_{0.75}Ga_{0.25}N$ photodiodes with low cutoff wavelength. Appl Phys Lett. 2006;88:123503.
9. Watschke L, Passow T, Fuchs F, Kirste L, Driad R, Rutz F, Leone S, Rehm R, Ambacher O. AlGaN avalanche Schottky diodes with high Al-content. Jpn J Appl Phys. 2019;58:SCCC11.
10. Reddy P, Breckenridge MH, Guo Q, Klump A, Khachariya D, Pavlidis S, Mecouch W, Mita S, Moody B, Tweedie J, et al. High gain, large area, and solar blind avalanche photodiodes based on Al-rich AlGaN grown on AIN substrates. Appl Phys Lett. 2020;116:081101.

11. Guo X, Rowland LB, Dunne GT, Fronheiser JA, Sandvik PM, Beck AL, Campbell JC. Demonstration of ultraviolet separate absorption and multiplication 4H-SiC avalanche photodiodes. IEEE Phot Tech Lett. 2006;18:136.

12. Zhou X, Han T, Lv Y, Li J, Lu W, Wang Y, Song X, Tan X, Liang S, Feng Z, Cai S. Large-area 4H-SiC ultraviolet avalanche photodiodes based on variable-temperature reflow technique. IEEE Elect Dev Lett. 2018;39:1724.

13. Liu H, McIntosh D, Bai X, Pan H, Liu M, Campbell JC, Cha HY. 4H-SiC pin recessed-window avalanche photodiode with high quantum efficiency. IEEE Phot Tech Lett. 2008;20:1551.

14. Vert A, Soloviev S, Fronheiser J, Sandvik P. Solar-blind 4H-SiC single-photon avalanche diode operating in Geiger mode. IEEE Phot Tech Lett. 2008;20:1587.

15. Bai XG, Guo X-Y, Mcintosh DC, Liu H-D, Campbell JC. High-detection sensitivity of ultraviolet 4H-SiC avalanche photodiodes. IEEE J Quantum Electron. 2007;43:1159.

16. Bai X, Liu H-D, McIntosh DC, Campbell JC. High-detectivity and high-single-photon-detection-efficiency 4H-SiC avalanche photodiodes. IEEE J Quantum Electron. 2009;45:300.

17. Zhou D, Liu F, Lu H, Chen D, Ren F, Zhang R, Zheng Y. High-temperature single photon detection performance of 4H-SiC avalanche photodiodes. IEEE Phot Tech Lett. 2014;26:1136–1138.

18. Xia Z, Zang K, Liu D, Zhou M, Kim T-J, Zhang H, Xue M, Park J, Morea M, Ryu JH, et al. High-sensitivity silicon ultraviolet p+-i-n avalanche photodiode by using ultra-shallow boron gradient doping. Appl Phys Lett. 2017;111:081109.

19. Shen P, Wraback M, Sampath AV, inventors; The United States of America as represented by the Secretary of the Army, assignee. Semiconductor photodetector with transparent interface charge control layer and method thereof. United States patent US 8,269,222. 2012.

20. Kwong NH, Rupper G, Binder R. Self-consistent T-matrix theory of semiconductor light-absorption and luminescence. Phys Rev B. 2009;79:155205.

21. Krishnamoorthy S, Nath DN, Akyol F, Park PS, Esposto M, Rajan S. Polarization-engineered GaN/InGaN/GaN tunnel diodes. Appl Phys Lett. 2010;97:203502.

22. Rajan S, Xing H, DenBaars S, Mishra UK. AlGaN/GaN polarization-doped field-effect transistor for microwave power applications. Appl Phys Lett. 2004;84:1591.

23. Lee LY. Cubic zincblende gallium nitride for green-wavelength light-emitting diodes. Mater Sci Tech. 2017;33(14):1570–1583. doi: 10.1080/02670836 .2017.1300726.

24. Rujirawat S, Wijewarnasuriya PS, Chen YP, Aqariden F, Sivananathan S. HgCdTe(211)B grown on CdTe(211)B/ZnTe(211)B/Si(211) by MBE. MRS Proc. 1996;450:281.

Appendix. Supporting Details

A.1 UV Light Nomenclature

UV radiation is defined as light with wavelengths between 10 and 400 nm, longer than 400 nm being the blue end of the visible light spectrum and shorter than 10 nm being the beginning of the X-ray region. Figure A-1 shows various spectral ranges and their names and also identifies two important plots. The black line represents the incident energy flux at sea level of light from the sun on a log-scale. The absorption of ionized gases and particle scattering help define the UVA, UVB, and UVC ultraviolet light ranges, while the terms near-, mid-, and far-UV are based on round numbers. With no UVC light reaching ground level, the term "solar-blind region" is often used to describe this region and, among early semiconductor device groups, as DUV. Besides 280 nm, defining the start of the solar-blind region, another important wavelength is 265 nm, the peak of the germicidal efficiency curve. Shown in purple on a linear scale in Fig. A-1, the germicidal efficiency curve represents the efficacy of light at different wavelengths to damage DNA and inhibit bacteria and (somewhat) virus replication. The short wavelength reduction in this curve results from absorption of light before reaching the cell nucleus and can be a function of the environment of interest.

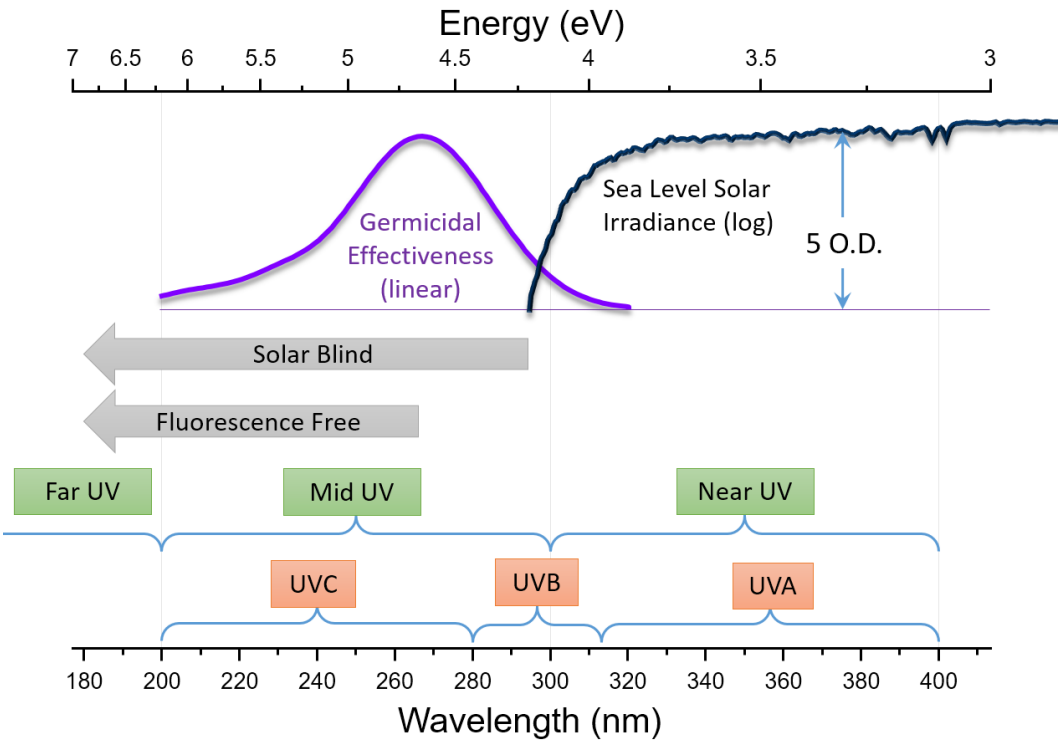

Fig. A-1 Terminology used in subdivision of the UV spectrum

List of Symbols, Abbreviations, and Acronyms

1-D	one-dimensional
3C-SiC	cubic silicon carbide
AlGaN	aluminum gallium nitride
AlN	cubic-aluminum-nitride
APD	avalanche photodiode
ARL	Army Research Laboratory
A/W	amps per watt
DEVCOM	US Army Combat Capabilities Development Command
DNA	deoxyribonucleic acid
DUV	deep-ultraviolet
EOMR	Electro-Optics Materials Research
FY	fiscal year
HRTEM	high-resolution transmission electron microscope
iCCD	intensified charge coupled device
I_{dark}	very low dark current
InGaN	indium gallium nitride
LED	light-emitting diode
MBE	molecular-beam epitaxy
NEGF	non-equilibrium Green's function
NUV	near-ultraviolet
PEQS	Photonics, Electronics & Quantum Sciences
PIC	photonic integrated chip
PL	photoluminescence
PNT	position, navigation, and time
PRIED	Portable Raman Improvised Explosive Detector
pW	picoWatt
QE	quantum efficiency
Q-PNT	quantum-precision navigation and timing
QW	quantum well

SACM	separate absorption, charge, and multiplication
SAM	separate absorption multiplication
SEDD	Sensor and Electron Devices Directorate
SiC	silicon carbide
SWaP-C	size, weight, power, and cost
TAC-BIO	Tactical Biological (detector)
TEM	transmission electron microscope/microscopy
TRPL	time-resolved photoluminescence
UV	ultraviolet
UVC	ultraviolet light with wavelengths between 200 and 280 nm

1 (PDF) DEFENSE TECHNICAL INFORMATION CTR DTIC OCA

1 (PDF) DEVCOM ARL
FCDD RLD DCI
TECH LIB

1 (PDF) DA HQ
DASA(R&T)

9 (PDF) USARMY AFC
L BROUSSEAU
R THYAGARAJAN
A LINZ
K WADE
S BRADY
J REGO
T KELLY
E JOSEPH
B SESSLER

2 (PDF) DEVCOM HQ
FCDD ST
C SAMMS
MJ HUBBARD

74 (PDF) DEVCOM ARL
FCDD RLC
C BEDELL
B SADLER
B PIEKARSKI
H EVERITT
FCDD RLC CA
L KAPLAN
FCDD RLC ES
G VIDEEN
S HILL
Y PAN
FCDD RLC I
B MACCALL
FCDD RLC N
BM RIVERA
A SWAMI
FCDD RLD
P BAKER
A KOTT
S SILTON
FCDD RLD D
T ROSENBERGER
FCDD RLD E
KS FOSTER
FCDD RLD F
K KAPPRA
FCDD RLD FR
M TSCHOPP
FCDD RLH
J CHEN
PJ FRANASZCZUK
JC LANE
K MCDOWELL
FCDD RLH B
JJ SUMNER
FCDD RLH F
JR GASTON
FCDD RLH T
D STRATIS-CULLUM
FCDD RLL
T KINES
FCDD RLL D
JS ADAMS
FCDD RLL DP
J MCCLURE
FCDD RLR
B HALPERN
S LEE
D STEPP
FCDD RLR E
RA MANTZ
C VARANASI
FCDD RLR EL
JX QIU
FCDD RLR EN
RA ANTHENIEN JR
FCDD RLR IC
MA FIELDS
SP IYER
FCDD RLR IM
JD MYERS
FCDD RLR IN
XN WANG
FCDD RLR
P REYNOLDS
FCDD RLR P
LL TROYER
FCDD RLR PC
D POREE
FCDD RLR PL
MK STRAND
FCDD RLS
J ALEXANDER
M GOVONI
M WRABACK
FCDD RLS C
M REED
FCDD RLS CC
S BEDAIR
FCDD RLS CE
TR JOW
CK XU

FCDD RLS CL
M DUBINSKIY
FCDD RLS E
RD DEL ROSARIO
FCDD RLS EA
A ZAGHLOUL
FCDD RLS ED
K JONES
G GARRETT
A SAMPATH
FCDD RLS S
WL BENARD
FCDD RLS SO
W ZHOU
FCDD RLW
SP KARNA
JF NEWILL
AM RAWLETT
SE SCHOENFELD
J ZABINSKI
FCDD RLW B
R BECKER
FCDD RLW M
ES CHIN
FCDD RLW S
V CHAMPAGNE
AL WEST
FCDD RLW T
RZ FRANCART
FCDD RLW TB
JD CLAYTON
FCDD RLW VB
A HALL
FCDD RLW W
TV SHEPPARD
FCDD RLW WA
B RICE
R PESCE-RODRIGUEZ
FCDD-SCT-TT
T PHAM